JACS
JOURNAL OF THE AMERICAN CHEMICAL SOCIETY

COMMUNICATION

pubs.acs.org/JACS

Cu^{2+}-Assisted Synthesis of Hexoctahedral Au−Pd Alloy Nanocrystals with High-Index Facets

Lei Zhang, Jiawei Zhang, Qin Kuang,* Shuifen Xie, Zhiyuan Jiang, Zhaoxiong Xie,* and Lansun Zheng

State Key Laboratory for Physical Chemistry of Solid Surfaces and Department of Chemistry, College of Chemistry and Chemical Engineering, Xiamen University, Xiamen 361005, China

Supporting Information

ABSTRACT: Controlled syntheses of multicomponent metal nanocrystals (NCs) and high-index surfaces have attracted increasing attention due to the specific physical and chemical properties of such NCs. Taking advantage of copper underpotential deposition as a bridge, hexoctahedral Au−Pd alloy NCs with {*hkl*} facets exposed were successfully synthesized, while phase separation occurred in the absence of Cu^{2+} ions. The as-prepared hexoctahedral Au−Pd alloy NCs exhibited very excellent performance in terms of both formic acid electro-oxidation and methanol tolerance due to synergism between the high-index facets and the alloy.

Noble metal nanocrystals (NCs) such as Au, Pd, and Pt have been widely applied in the fine chemicals industry and in energy conversion due to their high catalytic activity. Intensive studies have shown that the activity of these nanocatalysts closely depends on their size, shape, and composition.[1] Recently, multicomponent nanostructures, such as bimetallic (or trimetallic) hierarchical heterostructures,[2] core/shell structures,[3] and alloy structures,[4] have attracted increasing attention, as some specific physical and chemical properties (such as catalysis) could be enhanced by synergistic effects between different components. Among various multicomponent nanostructures, the synthesis of alloy NCs with a predetermined shape and composition is one of the most challenging tasks because of their distinct standard reduction potential (SRP) and atom sizes between different metals. Thermodynamically, two kinds of metals prefer to nucleate and grow separately in the wet-chemical synthetic process because of their different SRPs. To produce alloy NCs with desirable composition, one should ensure the simultaneous presence of solute metal atoms of all alloyed components at both nucleation and growth stages.[5] One feasible way to achieve this is to use strong reducing agents that can reduce simultaneously all metal precursors at proper rates.[6] Another way is to introduce specific surfactant or counterions, which can influence redox potentials of given metal ions through specific adsorption or coordination, making these ions be simultaneously reduced.[7] However, these methods are usually limited by the selection of appropriate metal precursors and surfactants, and sometimes phase separation cannot be avoided. Therefore, it remains a challenge to develop a new strategy for the synthesis of multicomponent alloy NCs. In addition, control over the surface structure of functional NCs, especially the control of high-index surfaces of metal-based NC, represents a new research trend in recent years. However, most research has focused on single metal phases rather than metal alloys and concerned successful control of high-index {*hk*0}, {*hkk*}, and {*hhl*} surfaces consisting of atomic steps.[3a−c,8] The {*hkl*} surfaces, which are composed of not only atomic steps but also kinks, are of much higher surface energy, and therefore more difficult to controlled. In the work described in this Communication, we employed underpotential deposition (UPD) of Cu on Au as a bridge to realize simultaneous reduction of Au and Pd, and we successfully prepared Au−Pd alloy NCs with a uniform size. The as-prepared Au−Pd alloy NCs possess a special hexoctahedral (HOH) shape enclosed by 48 {*hkl*} high-index facets, which is called the HOH Au−Pd alloy NCs for convenience. Such special HOH Au−Pd alloy NCs exhibited very excellent performance in terms of both formic acid electro-oxidation and methanol tolerance due to the synergism effect between the high-index facets and the alloyed atoms.

The HOH Au−Pd alloy NCs were prepared via a facile wet-chemical reduction route by using H_2PdCl_4 and $HAuCl_4$ as metal sources and L-ascorbic acid as reductant in the presence of octadecyl trimethyl ammonium chloride (OTAC) and copper(II) acetate ($Cu(CH_3COO)_2$) (see the Supporting Information for experimental details). Figure 1a shows a representative scanning electron microscopy (SEM) image of the as-prepared product, indicating that it is composed of well-shaped nanoparticles in high purity (>90%). These NCs are comparatively uniform in size, with an average size of 55 nm. By carefully surveying these NCs, one may find that they possess a hexoctahedral shape. The left column of Figure 1b shows high-magnification images of some NCs in different orientations. Although the outlines of these NCs are quite different, they can be matched by the same hexoctahedron projected from corresponding orientations, as shown by the schematic models in the right column of Figure 1b. Such a special hexoctahedron is enclosed by 48 {*hkl*} high-index facets, and it can be thought to be evolved from a tetrahexahedron with {*hk*0} surfaces[8a,9] by pushing the center of every square edge to the center (see Figure S1 in the Supporting Information). From the outlines of the HOH NCs, it was found that a hexoctahedron exposed with {431} facets (Figure 1b) could match well with the as-prepared Au−Pd alloy NCs. This structural feature was further confirmed by transmission electron microscopy (TEM), as shown in Figure 1c−e. Both

Received: July 8, 2011
Published: September 06, 2011

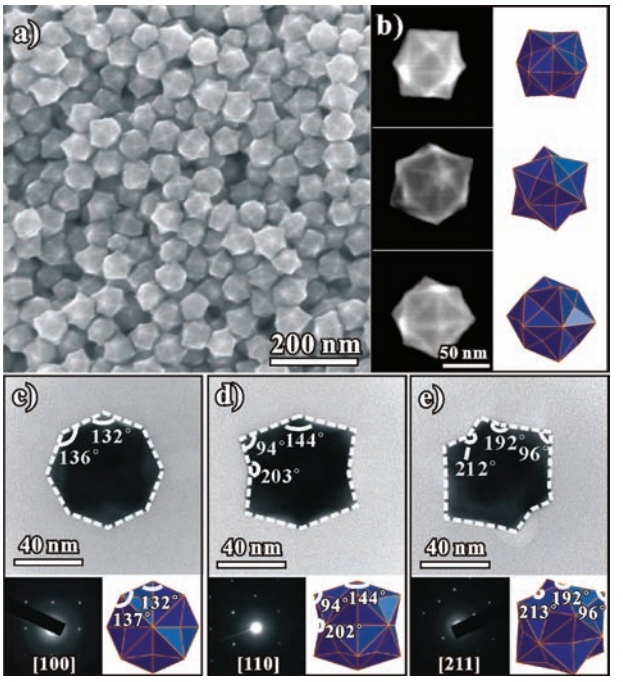

Figure 1. (a) SEM image of the as-prepared HOH Au−Pd alloy NCs. (b) A series of high-magnification SEM images and corresponding models of the HOH NCs with exposed {431} facets in different orientations. (c−e) TEM images, corresponding SAED patterns of the as-synthesized HOH Au−Pd alloy NCs, and schematic models of a hexoctahedron enclosed by the {431} facets oriented along the [100], [110], and [211] directions, respectively.

the outlines and angles between edges of an individual NC coincide well with the models of hexoctahedron bounded by {431} high-index facets when viewed from [100], [110], and [211] directions, respectively.

The composition of the as-prepared NCs was determined by X-ray powder diffraction (XRD). The XRD peaks of as-prepared HOH NCs can be indexed as face-centered cubic (fcc) structures, as shown in Figure 2a. Every diffraction peak appeared between the corresponding peak positions of pure fcc-structured Au and Pd, suggesting the successful formation of a Au−Pd alloy. The lattice parameter of the as-prepared HOH NCs was calculated to be 4.060(1) Å by the least-squares method. According to Vegard's law, which states that the crystal cell parameter of an alloy is linearly related to its composition,[10] the Pd content in our Au−Pd alloy can be determined as 11.1 ± 0.1%. This value is in agreement with the result of energy-dispersive X-ray spectroscopy (EDS) equipped on SEM, in which showed the molar ratio of Pd in Au−Pd alloy was about 12.8% (Figure S2). More definite compositional information was provided elemental mapping analysis by high-angle annular dark-field scanning transmission electron microscopy (HAADF-STEM)-EDS attached in the TEM. From the TEM image shown in Figure 2b, no obvious contrast change can be found for these HOH NCs, indicating that no core/shell or other heterostructures formed. Elemental mapping analysis (Figure 2c) demonstrates that the distribution ranges of Au and Pd are almost completely overlapped, although Au is much richer than Pd. On the basis of the above results, it can be concluded that the as-prepared HOH NCs are definitely Au−Pd alloy.

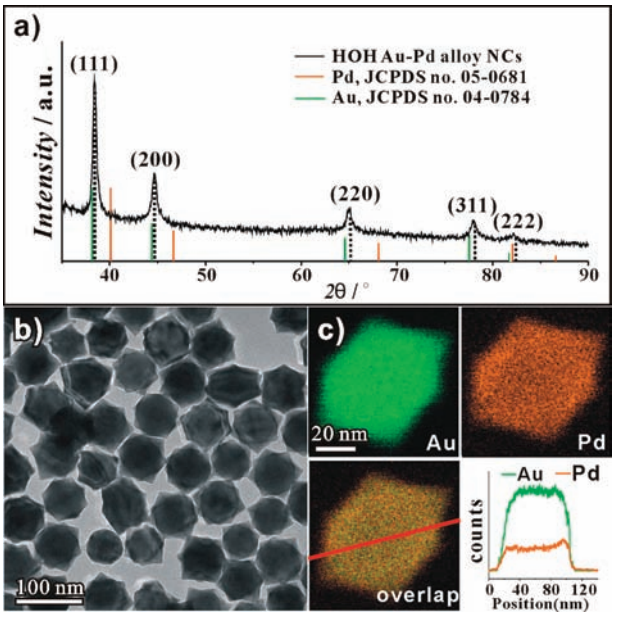

Figure 2. (a) XRD pattern and (b) TEM image of the as-prepared HOH Au−Pd alloy NCs. (c) Elemental scanning images and the cross-sectional compositional line-scanning profile of the Au−Pd alloy NCs.

It should be mentioned that the Pd content increases slightly from the core to the surface, as shown in compositional line-scanning profiles across the single NC. Time-dependent reaction experiments confirmed such a variation (Figure S3). It was found that the HOH rudimentary shape of the Au−Pd alloy formed as early as 1 h, and at that time the particle size was only 19 nm. With prolonging reaction time, the HOH shape of the Au−Pd alloy became more and more perfect, and the size of NCs gradually increased, reaching 55 nm at 12 h. The EDS analysis indicated that the Pd content also increased, from 8.2% to 12.8%, along with the reaction time (Figure S3h). Beyond 12 h, the Au−Pd alloy NCs tended to maintain a constant size and Pd content. Such a change in the Pd content could be due to different reduction ability of Au and Pd precursors, which results in different precursor concentrations during the reaction.

To probe the intrinsic factors influencing the formation of the HOH Au−Pd alloy NCs, a further series of control experiments were carried out. When no OTAC was added (i.e., only using pure ethylene glycol), porous Au−Pd alloy nanospheres of 50−100 nm size were produced, which were built up from tiny nanoparticles of just several nanometers (see Figure S4). However, irregular polyhedral particles were obtained in the OTAC aqueous solution (Figure S5). These results indicate that both OTAC and ethylene glycol act as capping agents to facilitate the formation of the special HOH shape. When the same molar amount of $CuCl_2$ was used instead of $Cu(CH_3COO)_2$, similar HOH alloyed NCs were synthesized (see Figure S6). The Pd content of the products was 11.9% measured by EDS analysis, which is similar to that of the products prepared with $Cu(CH_3COO)_2$. When neither $Cu(CH_3COO)_2$ nor $CuCl_2$ was added, the as-obtained product mainly consisted of irregular-shaped NCs of 60−80 nm, as shown in Figure 3a. A high-magnification SEM image shows that these irregular-shaped NCs always have some tiny nanoparticles of several nanameters size on the surface. The coexistence of two distinct nanostructures was also clearly observed by TEM (Figure 3b), and the two kinds

dx.doi.org/10.1021/ja2063617 |J. Am. Chem. Soc. 2011, 133, 17114–17117

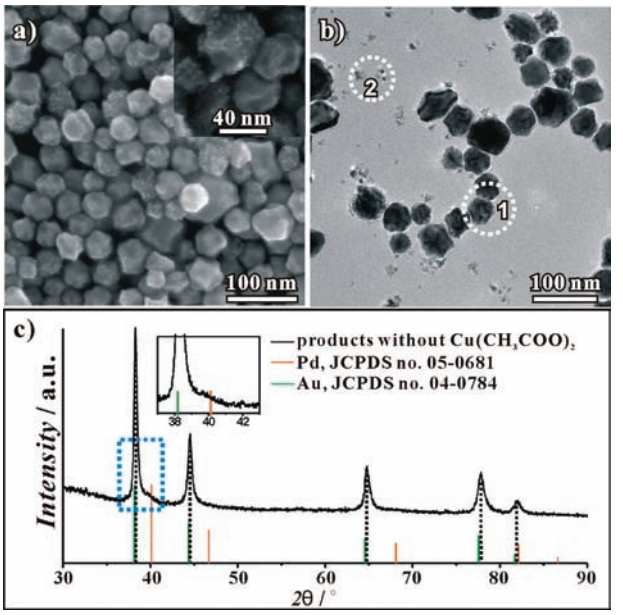

Figure 3. (a) SEM image, (b) TEM image, and (c) corresponding XRD pattern of the product obtained in the absence of $Cu(CH_3COO)_2$.

of nanostructures were found to possess different compositions by means of EDS attached on TEM. The large irregular polyhedral NCs (in zone 1 of Figure 2b) were composed of both Au and Pd, while those small nanoparticles (in zone 2 of Figure 2b) only contained Pd. Such a phase separation phenomenon was further confirmed by XRD characterization, as shown in Figure 3c. A set of very weak diffraction peaks assigned to fcc-structured Pd were detected at the positions marked by arrows in Figure 3c, accompanying the predominant diffraction peaks. Therefore, phase separation occurred, and the product obtained without using $Cu(CH_3COO)_2$ contained a small amount of tiny Pd nanoparticles. From the predominant diffraction peaks, a lattice parameter of 4.071(1) Å was calculated, which corresponds to 4.2 ± 0.1% Pd content in irregular polyhedral alloy NCs. The result indicated that the Pd content was remarkably reduced in the absence of Cu^{2+}. As a consequence, the presence of Cu^{2+} ions greatly improves the alloying of Pd into a Au lattice, which prevents the phase separation resulting from the different SRP between Au and Pd. In addition, the Cu^{2+} ions also play a key role in the formation of the HOH shape with the assistance of OTAC.

From the viewpoint of SRP (1.00 V for $AuCl_4^-$ and 0.59 V for $PdCl_4^{2-}$), $AuCl_4^-$ is usually reduced to metal before $PdCl_4^{2-}$ when they coexist, preferring to form the Au@Pd core−shell structure or hierarchical structure.[11] Our experiments demonstrate that addition of Cu^{2+} ions into the reaction system may have a great influence on the reduction process of Au and Pd. It is well known that Cu UPD occurs on the surface of Au substrate, and the redox potential of the Au/Cu(UPD) substrate is 150 mV more positive than that of $Cu^{+/0}$ (0.521 V);[12] it can be calculated to be 0.67 V. As the reduction potential of Cu UPD on a Au substrate is between those of $AuCl_4^-$ and $PdCl_4^{2-}$, Cu UPD on a Au surface should first occur before the reduction of $PdCl_4^{2-}$, which can serve as a bridge to induce the formation of Au−Pd alloy. On the basis of the above analysis, the following mechanism for the formation of the HOH Au−Pd alloy NCs is proposed: First, $AuCl_4^-$ is preferentially reduced because of its high reduction potential. A Cu UPD monolayer then deposits on the Au surface. As the reduction potential of $PdCl_4^{2-}$ is higher than the potential of $Cu^{2+/0}$ (0.341 V), $PdCl_4^{2-}$ may be reduced to Pd on the Au surface by galvanic replacement, and Cu atoms are reoxidized to Cu^{2+} ions. Simultaneously, the reduction of $AuCl_4^-$ may occur, and the Au−Pd alloy ultimately forms. With the help of Cu UPD, the difference between the SRPs of $AuCl_4^-$ and $PdCl_4^{2-}$ decreases, which benefits the formation of their alloy.

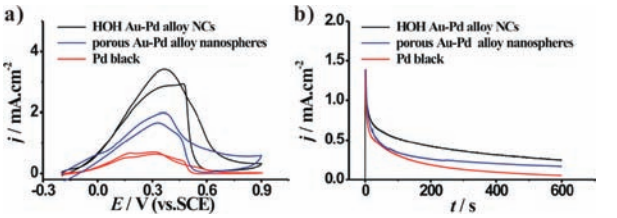

Figure 4. (a) CV curves measured on the as-prepared HOH Au−Pd alloy NCs, porous Au−Pd alloy nanospheres, and Pd black in an N_2-purged 0.50 M H_2SO_4 + 0.25 M HCOOH solution, respectively. Scan rate: 50 mV/s. (b) Current−time curves of formic acid oxidation measured on the three kinds of nanocatalysts in 0.50 M H_2SO_4 + 0.25 M HCOOH solution at 0.40 V. All current values were normalized with respect to the ECSA, and the current densities in electrocatalytic stability measurements have been normalized with respect to the initial value for the three samples.

Such a Cu UPD-assisted formation mechanism for Au−Pd alloy NCs can be confirmed by identifying the presence of a trace amount of Cu^0 in the HOH Au−Pd alloy NCs by X-ray photoelectron spectroscopy (XPS). Although no obvious Cu was found in the Au−Pd alloy NCs by the EDS technique, a weak binding energy peak at 931.7 eV was detected in the XPS spectrum, which should be assigned to Cu $2p_{3/2}$ of metallic Cu^0 (Figure S7). To further confirm the presence of Cu and determine the amount of each component in the HOH Au−Pd alloy NCs, the sample was analyzed by inductively coupled plasma atomic emission spectroscopy (ICP-AES). For the typical sample obtained at 12 h, the content of Au, Pd, and Cu in the HOH alloy NCs was 88.5%, 11.3%, and 0.2%, respectively, where the contents of Au and Pd are consistent with the EDS measurement. The ICP-AES detection results undoubtedly demonstrate that a trace amount of Cu did exist in the HOH Au−Pd alloy NCs. In fact, Cu UPD plays a key role not only in the formation of Au−Pd alloy but also in the formation of high-index facets of HOH NCs. The UPD process on the Au−Pd alloy particles' surface should affect the surface energy, which leads to the formation of {*hkl*} high-index facets. A similar effect has been reported in the Ag^+-mediated syntheses of Au NCs with a controlled shape.[13]

As there are high-density atomic steps and kinks on {*hkl*} high-index surfaces, the HOH Au−Pd alloys are expected to exhibit high chemical activity. Electrocatalytic oxidation of formic acid was used to characterize the catalytic activity of the as-prepared NCs. For comparison, the commercial catalyst Pd black and the porous Au−Pd alloy nanospheres obtained without OTAC (see Figure S4), as reference materials, were measured under the same conditions. Figure 4a shows cyclic voltammogram (CV) curves measured on glassy carbon electrodes loaded with the HOH Au−Pd alloy NCs, the porous Au−Pd alloy nanospheres, and Pd black, respectively, in a mixture of 0.50 M H_2SO_4 + 0.25 M HCOOH solution. It is found that the electrocatalytic ability of

dx.doi.org/10.1021/ja2063617 |*J. Am. Chem. Soc.* 2011, 133, 17114–17117

the porous Au−Pd alloy nanospheres is better than that of Pd black, suggesting that the alloy structure improves the electrochemical performance of the catalyst. Notably, the HOH Au−Pd alloy NCs with exposed {*hkl*} high-index facets is far superior to the porous Au−Pd NCs and Pd black. The oxidation current density measured on the HOH Au−Pd alloy NCs is almost 5 times that on Pd black. This result means that the {*hkl*} high-index facets consisting of high-density atomic steps and kinks indeed exhibit very high electrocatalytic activity. More importantly, the HOH Au−Pd alloy NCs also showed good stability in both catalytic performance (Figure 4b) and structure (Figure S8) during the electrochemical tests. Furthermore, the formation of Au−Pd alloy improves the methanol tolerance,[14] which is especially important for the application of the Pd-based catalysts in fuel cells (Figure S9). For the HOH Au−Pd alloy NCs, the hydrogen desorption peak, corresponding to the electrochemical active surface area (ECSA), was almost unchanged with or without methanol. By contrast, the ECSAs of the porous Au−Pd alloy nanospheres and Pd black decreased to 75.6% and 64.3%, respectively, when measured in the 0.10 M $HClO_4$ + 0.10 M CH_3OH solution. The high electrocatalytic ability of the HOH Au−Pd alloy NCs mainly originates from the synergism effect of the high-index facets and the Au−Pd alloy.

In summary, HOH Au−Pd alloy NCs with {*hkl*} high-index facets were synthesized by a facile wet-chemical method for the first time. Our experimental results demonstrate that the HOH Au−Pd alloy NCs exhibit good catalytic ability for formic acid electro-oxidation and methanol tolerance. Cu UPD was found to play a key role in formation of the HOH Au−Pd alloy NCs. Importantly, the proposed mechanism should be universal, and it is expected to have potential applications in preparing other bimetallic alloy nanostructures.

■ ASSOCIATED CONTENT

Supporting Information. Experimental details, schematic illustration for morphology evolution and EDS spectrum of the HOH Au−Pd NCs, time-dependent reaction results, SEM image and EDS spectrum of the product obtained in the presence of $CuCl_2$, XPS spectra of the HOH Au−Pd NCs, and results of electrochemical measurement in 0.10 M $HClO_4$ solution. This material is available free of charge via the Internet at http://pubs.acs.org.

■ AUTHOR INFORMATION

Corresponding Author
zxxie@xmu.edu.cn; qkuang@xmu.edu.cn

■ ACKNOWLEDGMENT

This work was supported by the National Basic Research Program of China (Grant Nos. 2011CBA00508 and 2007CB815303), the National Natural Science Foundation of China (Grant Nos. 20725310, 21021061, 21073145, and 21131005), and Key Scientific Project of Fujian Province of China (Grant No. 2009HZ0002-1).

■ REFERENCES

(1) (a) Jiang, Z. Y.; Kuang, Q.; Xie, Z. X.; Zheng, L. S. *Adv. Funct. Mater.* **2010**, *20*, 3634. (b) Sau, T. K.; Rogach, A. L.; Jäckel, F.; Klar, T. A.; Feldmann, J. *Adv. Mater.* **2010**, *22*, 1805. (c) Alayoglu, S.; Nilekar, A. U.; Mavrikakis, M.; Eichhorn, B. *Nat. Mater.* **2008**, *7*, 333. (d) Jin, M.; Liu, H.; Zhang, H.; Xie, Z.; Liu, J.; Xia, Y. *Nano Res.* **2011**, *4*, 83. (e) Tao, A. R.; Habas, S.; Yang, P. D. *Small* **2008**, *4*, 310. (f) Niu, W. X.; Xu, G. B. *Nano Today* **2011**, *6*, 265.

(2) (a) Lim, B.; Jiang, M.; Camargo, P. H. C.; Cho, E. C.; Tao, J.; Lu, X.; Zhu, Y.; Xia, Y. *Science* **2009**, *324*, 1302. (b) Peng, Z. M.; Yang, H. *J. Am. Chem. Soc.* **2009**, *131*, 7542. (c) Lee, H.; Habas, S. E.; Somorjai, G. A.; Yang, P. D. *J. Am. Chem. Soc.* **2008**, *130*, 5406.

(3) (a) Wang, F.; Li, C. H.; Sun, L. D.; Wu, H. S.; Ming, T.; Wang, J. F.; Yu, J. C.; Yan, C. H. *J. Am. Chem. Soc.* **2011**, *133*, 1106. (b) Lu, C. L.; Prasad, K. S.; Wu, H. L.; Ho, J. A.; Huang, M. H. *J. Am. Chem. Soc.* **2010**, *132*, 14546. (c) Yu, Y.; Zhang, Q. B.; Liu, B.; Lee, J. Y. *J. Am. Chem. Soc.* **2010**, *132*, 18258. (d) Wang, F.; Sun, L. D.; Feng, W.; Chen, H. J.; Yeung, M. H.; Wang, J. F.; Yan, C. H. *Small* **2010**, *6*, 2566. (e) Fan, F. R.; Liu, D. Y.; Wu, Y. F.; Duan, S.; Xie, Z. X.; Jiang, Z. Y.; Tian, Z. Q. *J. Am. Chem. Soc.* **2008**, *130*, 6949.

(4) (a) Zhang, L.; Zhang, J. W.; Jiang, Z. Y.; Xie, S. F.; Jin, M. S.; Han, X. G.; Kuang, Q.; Xie, Z. X.; Zheng, L. S. *J. Mater. Chem.* **2011**, *21*, 9620. (b) Yuan, Q.; Zhou, Z. Y.; Zhuang, J.; Wang, X. *Chem. Commun.* **2010**, *46*, 1491.

(5) Peng, Z. M.; Yang, H. *Nano Today* **2009**, *4*, 143.

(6) (a) Ferrando, R.; Jellinek, J.; Johnston, R. L. *Chem. Rev.* **2008**, *108*, 845. (b) Maksimuk, S.; Yang, S. C.; Peng, Z. M.; Yang, H. *J. Am. Chem. Soc.* **2007**, *129*, 8684. (c) Yang, S. C.; Peng, Z. M.; Yang, H. *Adv. Funct. Mater.* **2008**, *18*, 1.

(7) (a) Huang, X. Q.; Zhang, H. H.; Guo, C. Y.; Zhou, Z. Y.; Zheng, N. F. *Angew. Chem., Int. Ed.* **2009**, *121*, 4902. (b) Lee, Y. W.; Kim, M.; Kang, S. W.; Han, S. W. *Angew. Chem., Int. Ed.* **2011**, *50*, 3466.

(8) (a) Tian, N.; Zhou, Z. Y.; Sun, S. G.; Ding, Y.; Wang, Z. L. *Science* **2007**, *316*, 732. (b) Ma, Y. Y.; Kuang, Q.; Jiang, Z. Y.; Xie, Z. X.; Huang, R. B.; Zheng, L. S. *Angew. Chem., Int. Ed.* **2008**, *47*, 8901. (c) Zhang, J.; Langille, M. R.; Personick, M. L.; Zhang, K.; Li, S.; Mirkin, C. A. *J. Am. Chem. Soc.* **2010**, *132*, 14012. (d) Yu, T.; Kim, D. Y.; Zhang, H.; Xia, Y. *Angew. Chem., Int. Ed.* **2011**, *50*, 2773. (e) Huang, X. Q.; Zhao, Z. P.; Fan, J. M.; Tan, Y. M.; Zheng, N. F. *J. Am. Chem. Soc.* **2011**, *133*, 4718.

(9) Tian, N.; Zhou, Z. Y.; Sun, S. G. *J. Phys. Chem. C* **2008**, *112*, 19801.

(10) Denton, A. R.; Ashcroft, N. W. *Phys. Rev. A* **1991**, *43*, 3161.

(11) Lee, Y. W.; Kim, M.; Kim, Z. H.; Han, S. W. *J. Am. Chem. Soc.* **2009**, *131*, 17036.

(12) (a) Herrero, E.; Buller, L. J.; Abruña, H. D. *Chem. Rev.* **2001**, *101*, 1897. (b) Jennings, G. K.; Laibinis, P. E. *J. Am. Chem. Soc.* **1997**, *119*, 5208.

(13) (a) Kim, F.; Song, J. H.; Yang, P. D. *J. Am. Chem. Soc.* **2002**, *124*, 14316. (b) Tran, T. T.; Lu, X. M. *J. Phys. Chem. C* **2011**, *115*, 3638. (c) Grzelczak, M.; Pérez-Juste, J.; Mulvaney, P.; Liz-Marzán, L. M. *Chem. Soc. Rev.* **2008**, *37*, 1783. (d) Seo, D.; Park, J. C.; Song, H. *J. Am. Chem. Soc.* **2006**, *128*, 14863. (e) Ming, T.; Feng, W.; Tang, Q.; Wang, F.; Sun, L. D.; Wang, J. F.; Yan, C. H. *J. Am. Chem. Soc.* **2009**, *131*, 16350. (f) Chen, Y. H.; Hung, H. H.; Huang, M. H. *J. Am. Chem. Soc.* **2009**, *131*, 9114.

(14) Xu, C. X.; Zhang, Y.; Wang, L. Q.; Xu, L. Q.; Bian, X. F.; Ma, H. Y.; Ding, Y. *Chem. Mater.* **2009**, *21*, 3110.